Draft version October 10, 2022
Typeset using LaTeX **twocolumn** style in AASTeX63

PLANETESIMAL ACCRETION AT SHORT ORBITAL PERIODS

Spencer C. Wallace[1] and Thomas R. Quinn[1]

[1] *Astronomy Department, University of Washington, Seattle, WA 98195*

ABSTRACT

Formation models in which terrestrial bodies grow via the pairwise accretion of planetesimals have been reasonably successful at reproducing the general properties of the solar system, including small body populations. However, planetesimal accretion has not yet been fully explored in the context of more exotic terrestrial systems, particularly those that host short-period planets. In this work, we use direct N-body simulations to explore and understand the growth of planetary embryos from planetesimals in disks extending down to $\simeq 1$ day orbital periods. We show that planetesimal accretion becomes nearly 100 percent efficient at short orbital periods, leading to embryo masses that are roughly twice as large as the classical isolation mass. For rocky bodies, the physical size of the object begins to occupy a significant fraction of its Hill sphere at orbital periods less than about 50 days. In this regime, most close encounters result in collisions, rather than scattering, and the system cannot bifurcate into a collection of dynamically hot planetesimals and dynamically cold oligarchs, like is seen in previous work. The highly efficient accretion seen at short orbital periods implies that systems of tightly-packed inner planets should be almost completely devoid of any residual small bodies. We demonstrate the robustness of our results to assumptions about the initial disk model, and also investigate how far material can radially mix across the boundary between modes.

1. INTRODUCTION

Planetesimal accretion is a key phase in the terrestrial planet growth process, bridging the gap from kilometer-sized bodies up to roughly moon-sized objects known as planetary embryos. In the earliest stages of the planet formation process, aerodynamic forces dominate the growth and evolution of the solids and statistical models (Johansen et al. 2014; Birnstiel et al. 2016) are appropriate to describe how these numerous, small bodies coagulate. Due to the internal pressure support of the gas disk, the gas itself orbits at sub-Keplerian speed and exerts a headwind on any solids large enough to decouple from the gas (Weidenschilling 1977). Above about a meter in size, this headwind is maximally effective at sapping away angular momentum, and planet-building material can fall onto the central star on catastrophically short timescales (Weidenschilling 1977; Nakagawa et al. 1986). Additionally, laboratory experiments suggest that collisions between mm- to cm- sized solids tend to result in bouncing or destruction, rather than continued growth (Blum & Münch 1993; Beitz et al. 2011; Colwell 2003). For these reasons, a number of mechanisms which involve radially concentrating solids in a planet-forming disk have been proposed to facilitate fast growth from mm to km sizes (Johansen et al. 2007; Lyra et al. 2008; Bai & Stone 2010). Interestingly, formation models for the short-period multiplanet systems revealed by Kepler (Fabrycky et al. 2014) also seem to require enhanced concentrations of planet-building material to reproduce the observed architectures (Raymond et al. 2007; Hansen & Murray 2012).

Regardless of how the mm- to km-sized growth barriers are surmounted, gravity begins to dominate and aerodynamic gas drag plays a less significant role beyond this size. During this phase, collision cross sections are enhanced as gravitational focusing (Safronov 1969) acts to bend the trajectories of bodies undergoing close encounters. Because larger bodies are more effective at focusing the trajectories of nearby planetesimals, a period of runaway growth occurs (Wetherill & Stewart 1989; Kokubo & Ida 1996; Barnes et al. 2009). Eventually, the largest bodies (known as oligarchs) dynamically heat the surrounding planetesimals, severely limiting further growth (Kokubo & Ida 1998). The end result of this phase is a bimodal population of dynamically cold oligarchs, surrounded by dynamically hot, difficult to accrete residual planetesimals. Lines of evidence suggest that the asteroid belt, Kuiper belt and the Oort cloud are largely composed of the leftovers of this stage of planet formation.

After a long period of quiescence, the collection of embryos and remaining planetesimals undergoes a large-scale instability (Chambers & Wetherill 1998). As a consequence of the instability, the oligarchics are no longer on isolated, stable orbits and coalesce to form Earth-sized planets' through a series of extremely energetic, giant impacts (Kokubo & Ida 2002; Raymond et al. 2005, 2006).

Due to the relative ease of modeling the early dust coagulation phases and the final giant impact phase, these steps in the terrestrial planet formation process have received the most attention in the literature. The planetesimal accretion phase, which we will focus on in this paper, falls into an awkward in-between, where there are too many particles to directly track with traditional N-body codes, while the gravitational influence of the few, but massive oligarchs that form make statistical methods an inappropriate approach. Because of this limitation, planetesimal accretion is usually modeled in a narrow ring, and the results are then scaled to suit whatever situation is being studied. N-body simulations of terrestrial planet formation typically begin with a series of neatly spaced oligarchs, whose mass varies smoothly with orbital period. As we will show in this paper, this extrapolation with orbital period is inappropriate, particularly at short ($<$ 10 day) periods.

Given that systems of tightly-packed inner planets (STIPs) appear to be a common outcome of planet formation, understanding exactly how solids accumulate at short orbital periods is crucial. Although gas-disk driven migration of the planets themselves is often invoked to explain the observed architectures, we will focus on an in-situ model in this paper. That is, once the planetesimals themselves form, they largely stay in place and any subsequent large-scale movement of the solids are the result of mutual gravitational interactions. The focus of this work will be to understand how the outcome of the planetesimal accretion process scales with orbital period by using a high-powered N-body code to directly follow the growth and evolution of the planetesimals across a wide range of orbital periods (1 to 100 days). In doing so, we will assess whether the typical "isolation mass" initial conditions used in studies of terrestrial planet formation are actually appropriate for understanding STIPs. In a series of follow up papers, we plan to use these results to directly track the formation of full-sized planets from planetesimals and to understand how gravitational perturbations from a nearby gas giant might affect the outcome of this process.

In section 2 we provide an overview of the theory behind planetesimal accretion and show that assumptions used to derive the well-known modes of growth are only valid at sufficiently long orbital periods. We then motivate the need for N-body simulations to study this problem and describe the code used, along with how our initial conditions were constructed in section 3. In section 4, we present a parameter study of planetesimal accretion using a series of simulations of narrow annuli at various orbital periods. In section 5 we present a set of simulations starting with a much wider planetesimal disk and demonstrate that a transition between accretion modes occurs at moderately small ($\simeq$ 50d) orbital periods. Next, we assess the impact of simplifications made to our collision model on this result in section 6. In section 7, we discuss the implications of this multimodal accretion behavior throughout the disk for planet formation models and conclude.

2. OVERVIEW OF PLANETESIMAL ACCRETION

2.1. *Oligarchic and Runaway Growth*

We begin our analysis by considering a disk of equal planetesimals with radius r_{pl}, mass m_{pl} and surface density Σ_{pl}. The collision rate in the vicinity of an orbit defined by Keplerian frequency Ω can be written as $n\Gamma v$, where $n = \Sigma_{pl}\Omega/2m_{pl}v$ (where we have assumed that the scale height of the planetesimal disk goes as $\Omega/(2v)$. Γ describes the effective collision cross section and v is the typical encounter velocity between planetesimals. For a swarm of planetesimals on randomly oriented orbits, v is typically taken to the rms velocity, which can be related to the eccentricity and inclination distribution (e, i) in the following way (Lissauer & Stewart 1993):

$$\left\langle v^2 \right\rangle^{1/2} = \left(\frac{5}{4} \left\langle e^2 \right\rangle^{1/2} + \left\langle i^2 \right\rangle^{1/2} \right) v_k. \tag{1}$$

Assuming that every collision results in a perfect merger, the growth rate of a planetesimal is given by

$$\frac{dM}{dt} = \frac{\Sigma\Omega}{2m_{pl}}\Gamma. \tag{2}$$

In the case where the collision cross section, depends only on the physical size of the planetesimals, the growth scales linearly with mass and the mass distribution is expected to evolve in an "orderly" fashion. However, bodies larger than $\sim$ 100 km in size are expected to exert a significant gravitational force on each other during encounters and the collision cross section depends on both the size of the bodies and their encounter velocities. In this case, $\Gamma = \Gamma_{geo}\left(1 + v_{esc}^2/v^2\right)$ (Safronov 1969), where v_{esc} is the escape velocity from the two bodies at the point of contact.

In the limit that $v_{esc} \gg v$, it can be shown that $M \propto M^{4/3}$, which implies a runaway scenario, in which growth accelerates with mass. This mode of growth was confirmed with N-body simulations by Kokubo & Ida (1996) and appears necessary to construct protoplanets within the lifetime of a protoplanetary disk. Due to the velocity dependence of the gravitational focusing effect, it is not clear how ubiquitous this mode of growth is. In particular, encounter velocities at short orbital periods will be rather large (because $v \sim v_k$) and the $v_{esc} \gg v$ condition may not always be satisfied. The effect that a dynamically hot disk has on runway growth will be examined in detail in section 4.

An important feature is missing from the model described above, which limits its applicability at late times. Encounters between planetesimals that do not result in a collision play a crucial role over long timescales. These close encounters act to convert energy from Keplerian shear into random motion. Over time, this gravitational stirring effect will raise the typical encounter velocities between bodies and diminish the effectiveness of gravitational focusing. With a spectrum of masses, these velocity differences become even more pronounced because as the system evolves, it moves to a state of energy equipartition where $v \sim m^{1/2}$. For a system of equal mass bodies in which encounters are driven by random motions rather than Keplerian shear (dispersion dominated), the timescale for gravitational stirring is described by the two-body relaxation time (Ida & Makino 1993)

$$t_{relax} = \frac{v^3}{4\pi n G^2 {m_{pl}}^2 \ln\Lambda}, \tag{3}$$

where $\ln\Lambda$ is the Coulomb logarithm, typically taken to be ≈ 10 for a planetesimal disk. Despite the fact that the behavior of gravitational stirring is well-described by the two-body formalism, (Ida & Makino 1993) found that the stirring in a planetesimal disk is actually driven by close encounters. As we will show in section 4, gravitational stirring effectively shuts off when the Hill sphere of a body becomes comparable to its physical size. In this case, close encounters tend to result in collisions, and the main pathway for energy exchange between planetesimals is unable to operate.

As mentioned above, the system will tend toward a state of energy equipartition for a non-uniform mass distribution. Kokubo & Ida (1998) showed that runaway growth is actually self-limiting. As the runaway bodies grow larger, they become more effective at heating the remaining planetesimals, which diminishes the effectiveness of gravitational focusing and throttles the growth rate. Around the time that the mass of the runaway bodies exceeds the mass of the planetesimals by a factor of $\sim 50 - 100$ (depending on the orbital period) (Ida & Makino 1993) a phase of less vigorous "oligarchic" growth commences, in which the few largest bodies continue to accrete planetesimals at similar rates.

The picture described above relies upon an important assumption, which is that the mass distribution evolves slow enough for gravitational stirring to maintain energy equipartition. In other words, the relaxation timescale must remain short relative to the growth timescale. For typical conditions near the terrestrial planet forming region of the solar system, this timescale condition is satisfied. Due to the steep dependence of the relaxation time on encounter velocity, this condition can easily be violated at shorter orbital periods.

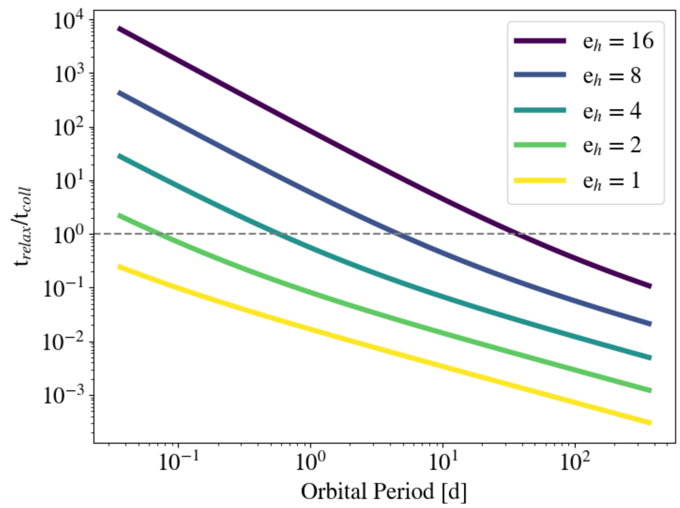

Figure 1. The ratio between the two-body relaxation and collision timescale for a population of equal-mass planetesimals with an internal density of 3 g cm^{-3} and an eccentricity dispersion characterized by e_h, where $e_h = 1$ is the boundary between shear and dispersion dominated encounters. Only in regions where $t_{relax} \ll t_{coll}$ can the velocity distribution respond to changes in the mass of the bodies such that oligarchic growth can operate. This condition is no longer satisfied for a dynamically hot disk at sufficiently short orbital periods.

In figure 1, we show ratio between the relaxation and collision timescale for a population of equal-mass planetesimals as a function of orbital period. Here, the encounter velocity is described by equation 1. For simplicity, we assume that $\left\langle e^2 \right\rangle^{1/2} = 2 \left\langle i^2 \right\rangle^{1/2}$ (Ida et al. 1993) and that the eccentricity dispersion is constant with orbital period. The eccentricity dispersion is described in units scaled by the Hill factor $(m_{pl}/3M_\star)^{1/3}$ such that $e_h = 1$ corresponds to the boundary between shear and dispersion dominated encounters. The horizontal dashed line indicates where $t_{relax} = t_{coll}$. The timescale criterion for oligarchic growth is only satisfied in regions where the disk is sufficiently dynamically cold and the orbital period is sufficiently long. In sections 4 and 5 we will explore the behavior and outcome of planetesimal accretion in regions where this criterion is *not* satisfied.

2.2. *Planetesimal Size and Extent of Hill Sphere*

In the formalism described above, the mass and velocity distribution of the bodies are both a function of time. Due to the interdependence of these quantities, it is not clear whether the timescales for gravitational scattering and growth will remain proportional as the oligarchs develop. In the case of many studies of planetesimal accretion in the solar system (cite examples), the $t_{relax} \ll t_{coll}$ condition must remain true, otherwise runaway growth would have continued until all of the planetesimals were consumed. However, it isn't immediately clear what will happen if the system begins in a state where $t_{coll} \ll t_{relax}$.

An insight into the expected behavior in this regime can be gained by defining the dimensionless parameter α, which is the ratio between the physical size of a body and it's Hill radius, r_h:

$$\alpha = \frac{r_{pl}}{r_h} = \frac{1}{a}\left(\frac{9M_\star}{4\pi\rho_{pl}}\right)^{1/3}, \quad (4)$$

where a is the semimajor axis of the body and ρ_{pl} is its bulk density. Assuming a fixed bulk density as bodies collide and grow, and that no large-scale migration occurs, the scaling of both r_{pl} and r_h with $m_{pl}^{1/3}$ means that α will be constant with time. For a composition of ice and rock, α is small for any populated region of the solar system ($\alpha \sim 10^{-2}$ for Earth and $\alpha \sim 10^{-4}$ in the Kuiper belt). As one moves close to the star α becomes larger than 1, which implies that the physical extent of a body exceeds its Hill sphere. (also mention that hill sphere size independent of velocity for small eccentricity)

The size of α controls the relative importance of gravitational scattering and collisions in driving the evolution of the planetesimal disk. In the case that α is small, most close encounters will result in a gravitational interaction only, moving the system toward a state of relaxation. If, however, the Hill sphere is largely filled by the body itself, these same encounters will instead drive evolution of the masses. Because α is independent of time, the innermost region of the planetesimal disk, where collisions dominate over scattering events, should remain that way.

We also introduce a second dimensionless quantity, which relates the physical size of the bodies to the velocity state of the system

$$\beta = \frac{r_{pl}}{r_g}. \quad (5)$$

where $r_g = Gm_{pl}/v^2$ is the gravitational radius of a body. Encounters between bodies inside of a distance of r_g result in significant deflections of their trajectories. It should be noted that the gravitational focusing enhancement factor v^2/v_{esc}^2 is equal to 1 for $\beta = 1$. In the case where r_g is smaller than the size of a planetesimal, the gravitational focusing enhancement factor will be between 0 and 1.

These scaling considerations motivate the range of parameters in the following numerical experiments as we explore the different regimes.

3. NUMERICAL METHODS

We use the tree-based N-body code ChaNGa[1] to model the gravitational and collisional evolution of planetesimals at short orbital periods (where α is large). ChaNGa is written using the CHARM++ parallel programming language and has been shown to perform well on up to half a million processors (Menon et al. 2015) and can follow the evolution of gravitationally interacting swarms of up to billions of particles. Using a modified Barnes-Hut tree with hexadecapole expansions of the moments to approximate forces, ChaNGa integrates the equations of motion using a kick-drift-kick leapfrog scheme. For all of the simulations presented in this paper, we use a node opening criteria of $\theta_{BH} = 0.7$. Additional information about the code is available in (Jetley et al. 2008; Menon et al. 2015).

Using the neighbor-finding algorithm in ChaNGa, originally designed for SPH calculations, we have recently implemented a solid body collision module in the code. This work is largely based on the solid-body collision implementation in PKDGRAV, which is described in Richardson (1994) and Richardson et al. (2000). To summarize, imminent collisions are detected during the "drift" phase by extrapolating positions of bodies forward in time, using the velocity calculated at the opening "kick". For each body, any neighboring particles which fall within a search ball of radius $2\Delta T v + 2r_{pl}$, where ΔT is the current timestep size for the particle and v is magnitude of its heliocentric velocity, are tested for an imminent collision. In the case that a collision is detected, the particles are merged into a single larger body, which is given the center of mass position and velocity of the two children. Resolving a collision can produce another imminent collision, so collisions are handled one-by-one and another full collision check is run after the previous event is resolved. For a more detailed description of the collision module in ChaNGa, see (Wallace & Quinn 2019). Particles are advanced in time on individual timesteps chosen as a power of two of a base timestep. The timestep for an individual particle is based on an estimate of the gravi-

[1] A public version of ChaNGa can be downloaded from http://www-hpcc.astro.washington.edu/tools/ChaNGa.html

tational dynamical time determined by the minimum of $\sqrt{d_{node}^3/(G(M_{node}+m_{pl}))}$ across all nodes in the tree that are accepted by the Barnes-Hut opening criterion. Here d_{node} is the distance from the planetesimal to the center of mass of the tree node and M_{node} is the total mass of the tree node. For nearby particles M_{node} is replaced with the mass of the nearby particle.

4. NARROW ANNULUS SIMULATIONS

We begin by presenting a parameter study of planetesimal accretion, motivated by two questions raised in section 2. 1) Does runaway growth still operate when the condition that $v \ll v_{esc}$ is not satisfied? 2) How does planetesimal accretion proceed when the planetesimals themselves occupy a significant fraction of their Hill spheres?

To answer these questions, we run a series of simulations in which a narrow annulus of planetesimals orbits a star. The values of α and β are varied individually. 4000 planetesimals with individual masses of 5×10^{23} g are placed with semimajor axes randomly drawn between 0.95 and 1.05 AU about a 1 $M_\odot$ star. The argument of perihelion ω, longitude of ascending node Ω, and mean anomaly M for each body is drawn from a uniform distribution $\in [0, 2\pi)$. The inclinations and eccentricities are drawn from a Rayleigh distribution with $\langle i^2 \rangle = 1/2 \langle e^2 \rangle$ (Ida et al. 1993).

In the "fiducial" case, we give the bodies a bulk density of 3 g cm^{-3}, and $\langle e^2 \rangle^{1/2} = 4e_h$, which corresponds to $\alpha = 3.6 \times 10^{-2}$ and $\beta = 3.4 \times 10^{-3}$. These parameters are chosen to match the initial conditions of Kokubo & Ida (1998), which gave rise to oligarchic growth. To vary the value of α, we alter the bulk density of the particles. In the high-α case, the bulk density is reduced by a factor of ~ 7100, which produces $\alpha = 1$. To vary β, the eccentricity dispersion is increased. For the high-β case, $\langle e^2 \rangle^{1/2}$ is increased to $1500e_h$, which corresponds to $\beta = 15,000$.

In all cases, the simulations are evolved with a base timestep of 1.7 days, which corresponds to 3% of an orbital dynamical time $\sqrt{a^3/GM_*}$. Due to the vastly differing growth timescales in each case, a simulation is stopped when the growth of the most massive body flattens out. In figure 2, we show the a-e distribution of bodies in the initial (blue) and final (orange) snapshots from each of the 4 simulations. The size of the points indicates the relative masses of the bodies. Only in the case of small α does a residual population of dynamically hot planetesimals develop. The lack of high eccentricity planetesimals in the large α case suggests that most encounters result in accretion instead of scattering. In the case of large β, the protoplanets and remaining planetesimals end up in a dynamically cool state, compared with the initial conditions. This is due to kinetic energy being lost as particles inelastically collide. One final point to note is the difference between eccentricities of the protoplanets in the large α, large β and the small α, large β case. The dynamically cooler result of the latter case is likely due to the dominant role that inelastic collisions play here.

In figure 3, we show the mass distribution of bodies from the final snapshot in each of the four cases. In addition to leaving fewer residual planetesimals, the large α simulations produce significantly larger embryos. Despite the vastly different encounter velocities of each population of bodies, the initial size of β (so long as bodies remain in the dispersion-dominated regime) appears to have no significant effect on the final distribution of masses.

To investigate whether any of these planetesimal rings underwent runaway growth, we examine the time evolution of the maximum and mean masses in each simulation. The ratio $m_{max}/\langle m \rangle$ is plotted in figure 4. On this plot, a positive slope indicates that the maximum and mean masses are diverging (i.e. the growth rate is accelerating with mass), which is evident for every case we have tested. Even with a large β, which means that the effective collision cross section is very near the geometric value, runaway growth still appears to operate. The ubiquity of the early positive trends in this figure indicates that, as bodies collide and grow the relative difference in gravitational focusing factors between bodies is what drives the system towards runaway growth. Although larger encounter velocities lengthen the growth timescales, this mode of growth appears to be inevitable, so long as gravity is the dominant force in the system. For the large α cases, the curves in this figure eventually turn over and begin to decline. Upon inspecting the simulation snapshots, we find that this trend is driven by an increase in the average mass as the planetesimal population becomes depleted. One should expect that the same thing will eventually occur for small α, although many more timesteps are required to begin to run out of planetesimals.

Additionally, these results suggest that the value of α, which is a function of only the initial conditions (the physical and Hill radius both scale with $M^{1/3}$, so α stays constant as bodies grow), controls the qualitative outcome of accretion. Across most of a planet-forming disk, α is small, and frequent gravitational encounters between the growing bodies will facilitate oligarchic growth. In the dispersion-dominated regime, close encounters drive the stirring between planetesimals and embryos (Weidenschilling 1989; Ida 1990). When α

Table 1. Summary of Full Disk Simulations Run

Name	m_{pl}^a	N_{pl}^b	A^c	α^d
fdHi	5×10^{22}	903,687	100	1.5
fdHiShallow	5×10^{22}	903,687	100	0.5
fdHiSteep	5×10^{22}	903,687	100	2.5
fdLo	5×10^{22}	45,185	1	1.5

Note
[a] Planetesimal mass [g]
[b] Number of planetesimals
[c] Solid surface density normalization (relative to MMSN)
[d] Solid surface density power law index

is large, the Hill sphere of a body is no longer mostly empty space, and close encounters that would otherwise result in stirring instead result in accretion. In this regime, we observe that runaway growth still commences, but nearly all of the planetesimals are swept up by the forming protoplanets, rather than being scattered onto higher eccentricity orbits, where they would otherwise remain as a remnant of the early stages of planet formation (Kokubo & Ida 1998, 2000).

5. FULL DISK SIMULATION

5.1. *Initial Conditions*

Motivated by the dependence of accretion modes on α, we next investigate whether this highly efficient, non-oligarchic growth should be expected to operate near the innermost regions of a typical planet-forming disk. Given that N-body simulations of short-period terrestrial planet formation typically begin with a chain of neatly-spaced, isolation mass (see Kokubo & Ida (2000) eq. 20) protoplanets, it is pertinent to determine whether the high α growth mode we revealed in the previous section invalidates this choice of initial conditions.

Given the dearth of short-period terrestrial planets observed around M stars (e.g. TRAPPIST-1), we chose to model the evolution of a series of wide planetesimal disks, which span from 1 to 100 days in orbital period, orbiting a late-type M star of mass 0.08 $M_\odot$. For a population of planetesimals with a bulk density of 3 g cm^{-3}, this orbital period range corresponds to $\alpha \in (0.7, 0.05)$. By simultaneously modeling a broad range of orbital periods, we can determine the critical value of α that divides these two modes of accretion, and also explore how the oligarchic/non-oligarchic accretion boundary affects the resulting distribution of protoplanets.

Four wide-disk simulations are run in total (see table 1). In each case, the solid surface density follows a power law profile

$$\Sigma(r) = \left(\frac{M_*}{M_\odot}\right) A\Sigma_{\rm MMSN} \left(\frac{r}{1\rm AU}\right)^{-\delta}, \tag{6}$$

where M_* is the mass of the central star, $\Sigma_{MMSN} = 10$ g cm^{-2} is surface density of the minimum-mass solar nebula (Hayashi 1981) at 1 AU, and A is an enhancement factor. In the first case (fdHi), we model a disk that follows a MMSN power law slope, with the overall normalization enhanced by a factor of 100. This choice of normalization for the solid surface density profile appears necessary in order to reproduce many observed short period terrestrial worlds in-situ (Hansen & Murray 2012). Additionally, we vary the power law index (fdHiShallow, fdHiSteep) and overall normalization (fdLo) of $\Sigma(r)$.

In all cases, the eccentricities and inclinations of the bodies are randomly drawn from a Rayleigh distribution, with $\langle e^2\rangle^{1/2} = 2\langle i^2\rangle^{1/2} = e_{eq}$. The value of e_{eq} is chosen such that the timescales for viscous stirring and aerodynamic gas drag on the planetesimals are in equilibrium. The viscous stirring timescale is given by Ida & Makino (1993) as

$$\tau_{vs} = \frac{\langle e^2\rangle}{d\langle e^2\rangle/dt} \approx \frac{1}{40}\left(\frac{\Omega^2 a^3}{2Gm_{pl}}\right)^2 \frac{4m_{pl}\langle e^2\rangle^2}{\Sigma a^2\Omega}, \tag{7}$$

where Ω, a and e are the orbital frequencies, semimajor axes and eccentricities of the individual planetesimals. In the Stokes regime, the gas drag timescale is given by Adachi et al. (1976) as

$$t_s = \frac{2m_{pl}}{C_D \pi r_{pl}^2 \rho_g v_g}, \tag{8}$$

where C_D is a drag coefficient of order unity, ρ_g is the local gas volume density and v_g is the headwind velocity of the gas experienced by the planetesimal. The local gas volume density is given by

$$\rho_g = \frac{\Sigma_g}{\sqrt{2\pi}h_g \exp\left[-z^2/\left(2h_g^2\right)\right]}, \tag{9}$$

where Σ_g is the gas surface density (taken to be 240 times the solid surface density), $h_g = c_s/\Omega$ is the local gas scale height and z is the height above the disk midplane. The sound speed profile is given by $c_s = \sqrt{k_B T(r)/(\mu m_H)}$, where k_B is Boltzmann's constant, $T(r) = T_0 r^{-Q}$, $\mu = 2.34$ and m_h is the mass of a hydrogen atom. For a protoplanetary disk around a typical M star, $T_0 = 148$ K and $Q = 0.58$ (Andrews & Williams 2005).

Finally, the headwind velocity of the gas, due to the fact that the gas disk is pressure supported, is given by

$$v_g = v_k\left[1 - \sqrt{Qc_s^2/v_k^2}\right], \tag{10}$$

where v_k is the local Keplerian velocity. As in section 4, the argument of perihelion ω, longitude of ascending node Ω, and mean anomaly M for the planetesimals are drawn from a uniform distribution $\in [0, 2\pi)$.

5.2. *Gas Drag Force*

In addition to the mutual gravitational forces, a Stokes drag force from to the gas disk is applied to each particle, following the prescription described in section 2.2.1 of Morishima et al. (2010).

5.3. *Timestepping Criterion*

In the case of the fdHi simulation, there are nearly 1 million particles, whose orbital periods vary by two orders of magnitude. Because the interaction timescales near the inner edge of the disk are exceedingly short, a fixed timestep size would required a prohibitively large number of steps to follow planetesimal growth throughout the entire disk. For this reason, we use a multi-tiered timestepping scheme, in which particles are placed onto the nearest power of two timestep based on their most recently calculated gravitational acceleration. [2]

This more efficient scheme introduces two issues, however. Firstly, momentum is not completely conserved when bodies switch timesteps. The error introduced becomes particularly severe for a particle on an eccentric Keplerian orbit, whose perihelion and aphelion distances straddle a timestep boundary. For a large collection of particles, this problem manifests itself as the development of a V-shaped gap in the semimajor axis-eccentricity plane, which is centered on the boundary itself. To correct this problem, we introduce a slightly modified timestepping criterion, which is based on the expected gravitational acceleration of the particle at pericenter. Only in the case of a close encounter with another planetesimal (in which the acceleration is no longer dominated by the star) is the timestep allowed to reduce based on the original criterion.

A second issue is introduced when two particles on different timesteps undergo a collision. As in the previous case, momentum is not completely conserved because the most recent 'kick' steps did not happen simultaneously for these bodies. Early in the simulation, we find that runaway growth tends to initiate at the timestep boundaries. This issue carries itself forward through the embryo formation phase, and protoplanets tend to form at the boundaries. To correct this issue, we ignore collisions between bodies on different timesteps early in the simulation. We find that preventing multi-timestep collisions until after the maximum mass grows by a factor of 10 prevents any artifacts from developing at the timestep boundaries, while also minimizing the number of 'skipped' collisions[3].

[2] This scheme is used on almost all works using ChaNGa, and is common among large-scale simulation codes.

Table 2. Final Properties of Full Disk Simulations

Name	M_{PP}^a	T_{int}^b	T_{int1}^c
fdHi	1.00	456	16,377
fdHiShallow	1.19	456	16,377
fdHiSteep	1.08	456	16,377
fdLo	1.77×10^{-3}	3,713	133,651

Note
[a] Maximum protoplanet mass [M_{earth}]
[b] Integration time [yr]
[c] Rescaled integration time [yr]

5.4. *Results*

The timescales for embryo formation depend on the chosen surface density profile, along with the local orbital timescale. Protoplanets form first at the inner edge of the disk, where the dynamical timescales are short. Growth proceeds in an inside-out fashion, with the outermost regions of the disk completing the protoplanet assembly phase last. This radial timescale dependence is not typically accounted for in planet formation simulations[4], and appears to be an important component to forming realistic solar system analogs (Clement et al. 2020). As with the narrow annulus simulations, we stop the integration once the masses of protoplanets in the outermost region of the disk reach a steady value. In table 2, we summarize the outcomes of the four "full disk" cases.

We show the final state of the "fdHi" simulation in figure 5. In the top panel, the initial (contours) and final (points) state of the simulation is shown in the orbital period-eccentricity plane. The size of the points indicates the relative mass of the bodies. In the bottom panel, the mass of the largest bodies is shown as a function of orbital period. The solid curves indicate the isolation mass,

$$M_{iso} = \left[\frac{\left(2\pi a^2 \Sigma \tilde{b}\right)^3}{3M_*} \right]^{1/2}, \tag{11}$$

[3] In the case of fdHi, only about 20 collisions out of an eventual 900,000 are ignored.

[4] Instead, the innermost protoplanets patiently 'wait' for this phase of evolution to complete everywhere in the disk

where $\tilde{b}$ is the size of the feeding zone in units of Hill radii. For two bodies on circular, non-inclined orbits, $\tilde{b} = 2\sqrt{3}$ is the smallest orbital separation that produces a non-negative Jacobi energy and permits a close encounter (see Nakazawa & Ida (1988)). In typical oligarchic growth simulations (Kokubo & Ida 1998), protoplanets tend to space themselves apart by $\tilde{b} = 10$ (although it should be noted that they do not consume all of the planetesimals within this distance). The isolation mass is plotted in blue and orange for these two values of $\tilde{b}$, respectively.

A qualitative shift in the protoplanet and planetesimal distribution is visible at ~ 60 days. Interior to this location, there are very few remaining planetesimals and the embryos formed are noticeably more massive. Protoplanets in this region appear to closely follow the isolation mass curve for $\tilde{b} = 10$. Exterior to the boundary, the residual planetesimal population is much more pristine, and protoplanets more closely follow the $\tilde{b} = 2\sqrt{3}$ curve. This suggests that the transition between the low α and high α accretion modes seen in section 4 happens near this location.

In section 4, we postulated that the increased importance of inelastic damping in the inner, non-oligarchic growth region of the disk should lower the overall eccentricity of the protoplanets there. This behavior is not immediately apparent in the top panel of figure 5. There are, however, a couple of factors in the wide disk simulations that could make this extra dynamical cooling mechanism difficult to see. Firstly, the initial eccentricity distributions of the inner and outer disk are different because of the dependence of the viscous stirring and gas drag timescales on orbital period. Additionally, the protoplanet formation timescales for the inner and outer disk are vastly different, making a comparison between these regions at the same moment in time somewhat inappropriate.

To ensure that the boundary seen near 60 days in orbital period is not simply a transient product of the inside-out growth throughout the disk, we examine the time evolution of σ/Σ at multiple orbital periods. In figure 6, the value of σ/Σ is plotted as a function of time in 10 orbital period bins, each with a width of 10 days. Bins interior to 60 days are shown by a dashed line, while those exterior are shown as a solid line. In all radial bins, the planetesimal surface density is approaching an asymptotic value. In the inner disk, this value asymptotes to zero as the planetesimal population entirely depletes. In the outer disk, dynamical friction between the embryos and planetesimals eventually throttles subsequent accretion and leaves ~ 10 percent or more of the mass surface density as planetesimals. It should be noted that in a typical oligarchic growth scenario, where protoplanets space themselves apart by 10 r_h and settle onto circular orbits (giving $\tilde{b} = 2\sqrt{3}$), roughly 30 percent of the planetesimal mass should remain out of reach of the protoplanets.

Next, we investigate how the resulting planetesimal and protoplanet distribution changes as we vary the initial solid surface density profile. The final orbital period-eccentricity state of the particles in the fdHi, fdHiSteep, fdHiShallow and fdLo simulations are shown in figure 7, with point sizes indicating the relative masses of the bodies. In all cases, the inner disk is largely depleted of planetesimals, while the outer disk contains a bimodal population of planetesimals and embryos, with a clear separation in eccentricity between the two. Despite having significantly different masses, the planetary embryos formed in all simulations have remarkably similar eccentricities. This is likely due to the fact that inelastic collisions play a more significant role where the solid surface density is highest, which offsets the fact that the initial bodies started off in a dynamically hotter state.

In figure 8, we plot the masses of the resulting protoplanets and planetesimals in all four simulations in units of $\tilde{b}$ (see equation 11). Here, we assume that each embryo has reached its isolation mass, and that differences in mass are driven by differences in the initial surface density at the embryo's current location, along with the size of its feeding zone, which is set by the dynamics relevant at that location in the disk. By plotting the derived value of $\tilde{b}$ as a function of orbital period, differences in the dynamical interactions at different locations of the disk are made more clearly visible. As mentioned previously, $\tilde{b} = 2\sqrt{3}$ (indicated by the horizontal dashed line) carries a special significance, being the minimum feeding zone width that a body can have. In all four simulations, the feeding zone width exceeds the minimum value in the inner disk and approaches $2\sqrt{3}$ beyond ~ 60 days. The orbital periods at which this transition occurs are quite similar between simulations, despite the vastly different solid surface density profiles used. This indicates that the boundary between accretion modes is not dependent upon the surface density profile chosen, and also supports our conclusion that planetesimal accretion is largely complete everywhere in the disk.

5.5. *Assembly History of Embryos*

Further insight regarding the difference between the short vs long period accretion modes can be gained by looking at the merger history of the planetary embryos. Because all collisions are directly resolved by the N-body code, a direct lineage can be traced between the resulting planetary embryo and the initial planetesimals.

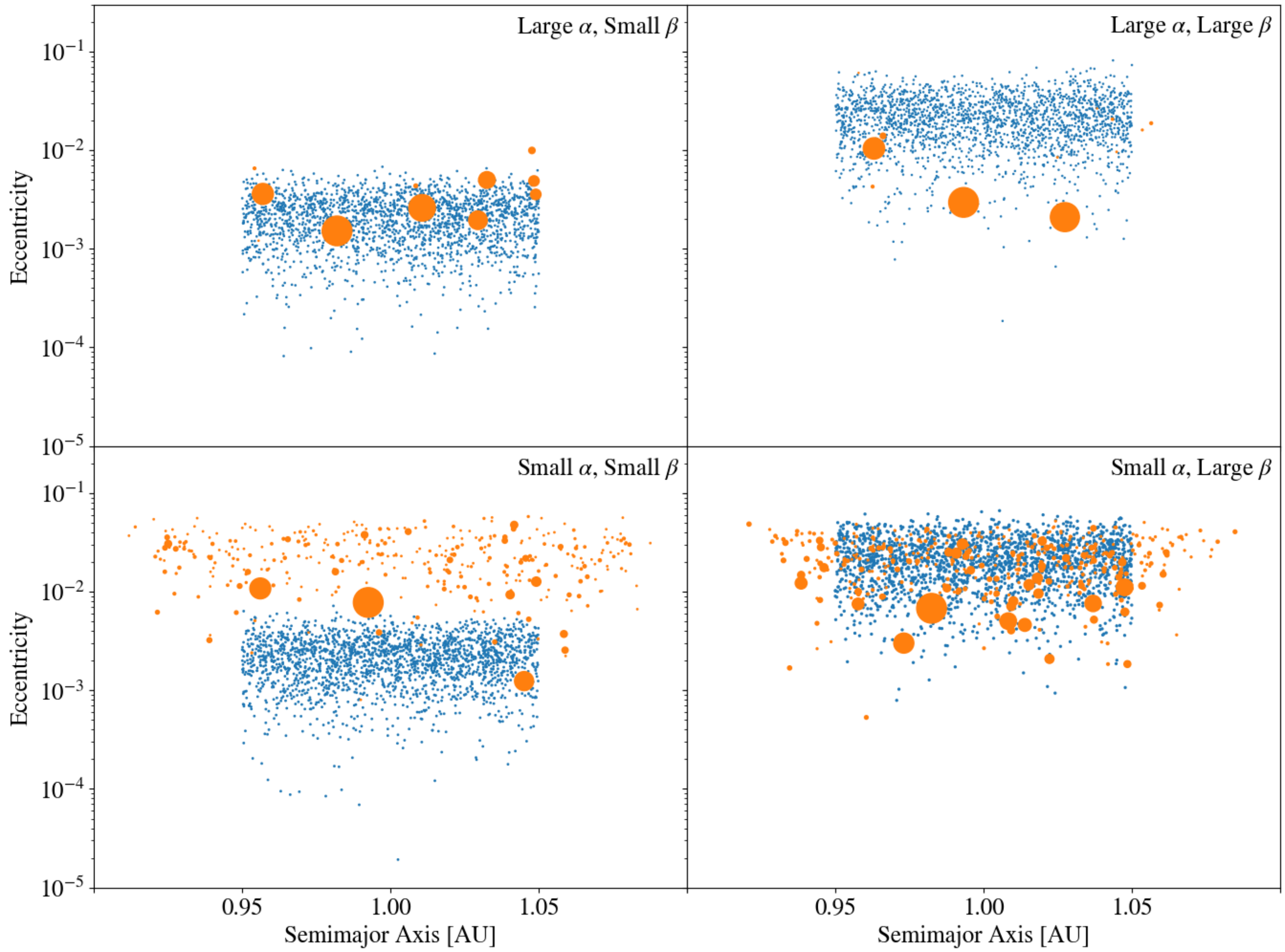

Figure 2. The initial (blue) and final (orange) states of the simulations described in section 4. Relative masses of the bodies are indicated by point size. In the case of large α, almost no residual planetesimal population remains. Regardless of the initial choice of β, the protoplanets that form attain similar eccentricities.

We begin by investigating the "smoothness" of the accretion events that give rise to each embryo. Drawing from a common technique used for cosmological simulations of galaxy formation, we divide growth events for a given body into "major" and "minor" mergers. Here, we define minor events as any collision involving an initial mass planetesimal, while major events consist of a merger between any two larger bodies. In figure 9, we choose the 100 largest bodies at the end of the fdHi simulation, retrieve all collision events involving these bodies, and plot the total mass fraction attained through minor events as a function of the final mass of the body. The bodies are then subdivided into those that end up with orbital periods greater than 60 days (red x's) and less than 60 days (blue dots). For the bodies in the outer oligarchic growth region, the trend between smooth accretion mass fraction and final mass is nearly flat. Regardless of how much an embryo has grown, mergers with initial mass planetesimals contribute on the order of a few percent to the final mass. At shorter orbital periods, however, the contribution from minor mergers can be over an order of magnitude smaller as the embryos mature.

The variation in smooth accretion fraction with mass for the short period bodies suggests that the planetesimal and embryo populations interact differently than those in the outer disk. Exterior to the 60 day accretion mode boundary, the growing embryos continue to accrete planetesimals as they near their final mass. Inside the boundary, however, later growth events tend to be dominated by embryo-embryo collisions, and the smooth accretion fraction drops as mergers with planetesimals play a less significant role. As we discussed in section 2.2, gravitational scattering should be very

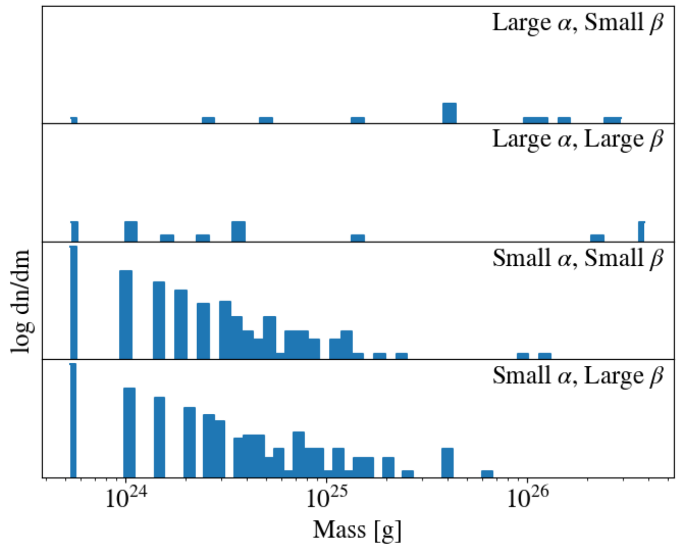

Figure 3. The final state of the mass distribution for the simulations described in section 4. For small α, a few embryos form alongside a power law tail of planetesimals. For larger values of α, the mass distribution takes on a more uniform form. As in the previous figure, the initial choice of β does not appear to have any meaningful impact on the end result.

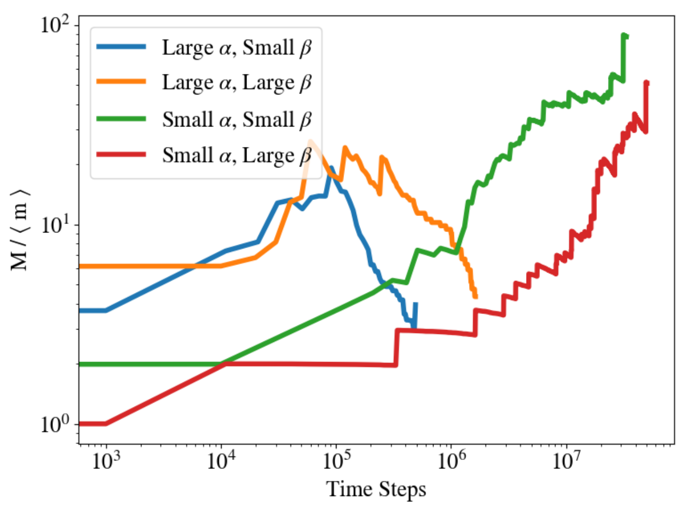

Figure 4. The evolution of the ratio between the maximum and mean mass for the four simulations presented in section 4. The runaway growth phase can be identified by a positive slope in this ratio. For all values of α, an increase in β has the effect of delaying the growth of the embryos.

weak in the inner disk. Gravitational scattering between embryos and planetesimals is a key ingredient for orbital repulsion (see Kokubo & Ida (1998)), and so a lack of gravitational scattering should prevent the embryos from settling onto neatly-spaced, isolated orbits. As we

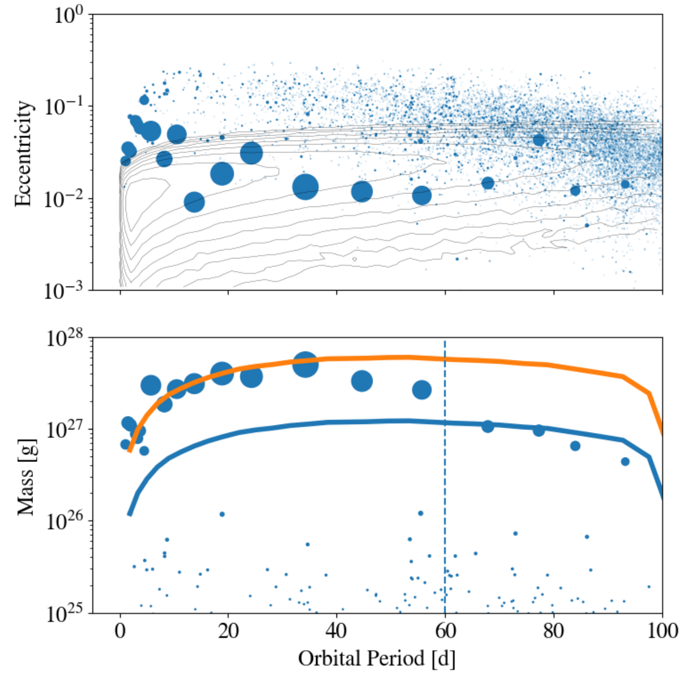

Figure 5. The final state of the fdHi simulation. In the top panel, the contours denote the initial period-eccentricity distribution of the planetesimals. Point sizes indicate the relative masses of bodies. In the bottom panel, the solid line indicates the isolation mass for $\tilde{b} = 2\sqrt{3}$. The vertical dashed line marks the approximate location of the accretion mode boundary. For $P_{orb} < 60$ days, the high α accretion mode produces embryos that exceed the isolation mass.

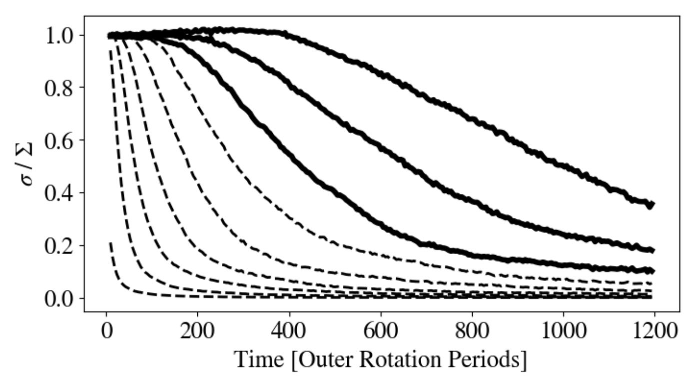

Figure 6. The time evolution of the planetesimal surface density (in units of the total solid surface density) in the fdHi simulation. Each curve represents a radial slice of the disk. The innermost region evolves the quickest, and is therefore represented by the lowest curve. The dashed lines indicate radial zones interior to the 60 day orbital period boundary.

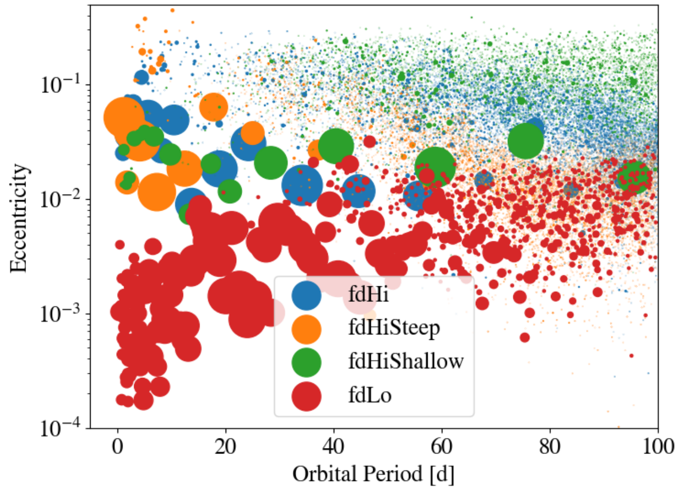

Figure 7. The final state of all simulations listed in table 2. Point sizes indicate mass relative to the largest body in the fdHi simulation.

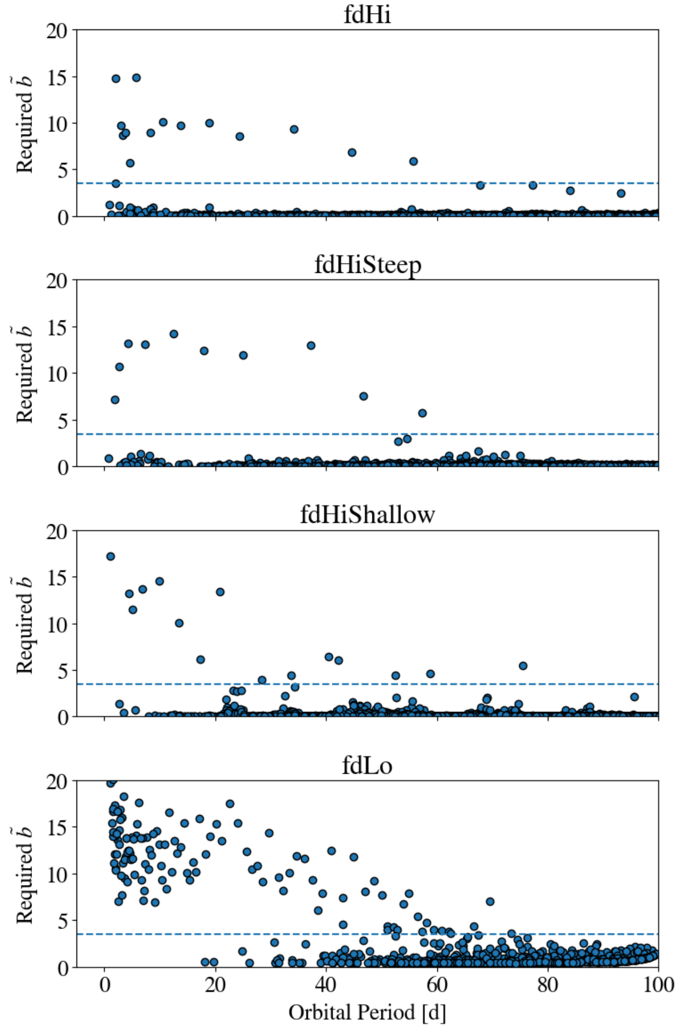

Figure 8. Feeding zone width (see equation 11 required to produce the final masses for the protoplanets from the simulations listed in table 2. The horizontal dashed line indicates $\tilde{b} = 2\sqrt{3}$. Despite the vastly different initial solid surface density profiles, the feeding zone width reaches the circular orbit value around ~ 60 days.

showed in figure 8, the embryos in the inner disk appear to reach well beyond the typical feeding zones predicted by an oligarchic growth model. Figure 9 suggests that this extra mass here obtain comes from mergers with the other nearby embryos.

Another line of evidence pointing to a lack of gravitational scattering and orbital repulsion in the inner disk can be seen in figure 10. Here, we have chosen the 20 most massive bodies from the fdHi simulation and arranged them in order of final orbital period. On each line, the black has mark indicates the present orbital period of an embryo and the gray histogram represents the initial orbital period distribution of the planetesimals which were used to construct the embryo. One should note that unlike the previous figure, this plot shows where every single bit of mass (in the form of planetesimals) originated, rather than only denoting embryo-planetesimal collisions.

Qualitatively, there are a couple of differences between the initial planetesimal distributions in the inner (< 60 days) and outer (> 60 days) part of the disk. The planetesimal distributions for the outer disk are much more smooth and unimodal, while many of the distributions near the inner disk have multiple peaks. As we discussed when examining figure 9, growth events for the inner embryos tend to be sudden and stochastic, often involving pairs of embryos. When an embryo-embryo collision happens, one would expect a second peak to appear in the accretion distribution as the merger tree suddenly obtains a whole other subtree from the embryo that it absorbed. In the outer disk, however, the increased importance of embryo-planetesimal mergers means that growth should be smooth, steady and local.

In figure 10, evidence of orbital repulsion can be seen for the outermost embryos. Beyond 60 days, the final positions of the embryos tend to be offset from the peaks of the accretion distributions. This suggests that gravitational scattering events between embryos occurred later on, after accretion had mostly completed. Although many of the inner embryos also end up shifted away from the peak of their accretion distribution, their present position is usually associated with another secondary peak. This suggests that most of the close en-

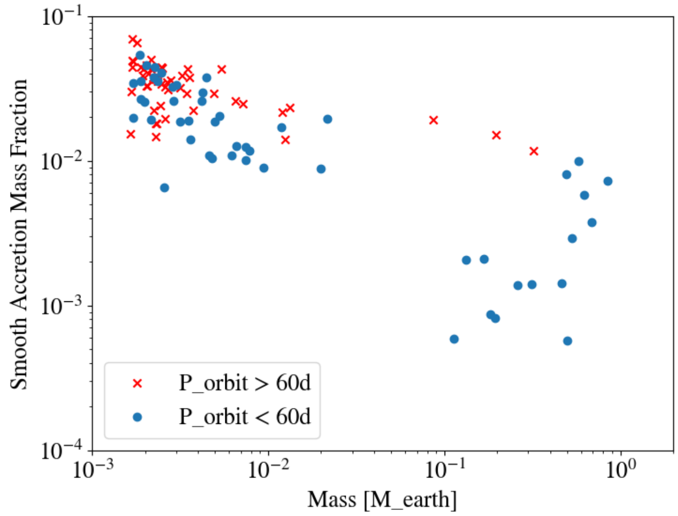

Figure 9. For the 100 most massive bodies at the end of the fdHi simulation, the fraction of their total mass attained through mergers with initial mass planetesimals (smooth accretion) as a function of total mass. Bodies that reside beyond the 60 day accretion boundary are shown with red crosses, while bodies interior to the boundary are shown with blue dots. For the short period bodies, there is a decreasing correlation between smooth accretion fraction and mass, which suggests that most growth occurs between equal mass bodies. For the longer period bodies in the oligarchic growth region, this trend is flat, indicating that accretion of planetesimals is important during all phases of evolution.

counters between embryos here resulted in a merger event, rather than a scatter.

6. SIMPLIFYING ASSUMPTIONS

6.1. *Collision Cross Section*

In all cases shown so far, the boundary between the standard oligarchic growth and the highly-efficient short period accretion region lies around 60 days in orbital period. The mode of accretion is set entirely by the local value of α, which scales with both distance from the star and the bulk density of the planetesimals (see equation 4). The artificial inflation of the collision cross section of the particles in our simulations, which is meant to reduce the computational expense, has the side effect of reducing the bulk densities. Because $\alpha \sim \rho_{pl}^{-1/3}$, increasing the particle sizes by a factor of $f = 6$ reduces the orbital period at which α has a given value by a factor of approximately 15. Therefore, one would expect the accretion boundary to lie near 5 days in orbital period for 3 g cm^{-3} bodies.

Although a simulation with $f = 1$ is not computationally tractable, we can test whether the accretion boundary moves in the way we expect by modestly changing the value of f. In figure 11, we compare the fdHi simulation to a nearly identical run using $f = 4$. In the top panel, the embryo masses in units of the isolation mass are shown as a function of orbital period. In the bottom panel, the value of α as a function of orbital period is shown for 3 g cm^{-3} bodies with an artificial radius enhancement of $f = 1$, 4 and 6. The horizontal dashed line indicates the value of alpha below which the accretion mode switches to oligarchic growth. Comparing the top and bottom panels, the intersection of the embryo masses and local isolation mass matches well with the orbital period at which $\alpha \sim 0.1$. Also shown by the shaded region are α values for realistic sized bodies with ρ_{pl} between 1 and 10 g cm^{-3}. In all cases, the accretion boundary still lies within the part of the disk in which solids would be expected to accumulate (citation?).

6.2. *Collision Model*

In the simulations presented in this work, all collisions result in a complete merging of a pair of bodies with no loss of mass or momentum. Although simple to model, this assumption of perfect accretion may result in overly efficient growth, particularly at the innermost region of the disk where encounter velocities are the largest. To handle this issue properly, semianalytic collision resolution models have been developed and implemented in N-body codes (see Leinhardt & Stewart (2012)). However, resolving collisional debris fragments using a direct approach as we have done with ChaNGa would result in an intractably large number of particles.

To test whether a more restrictive collision model should modify our results, we present a smaller scale test using a slightly more sophisticated collision model. In this case, a collision can result in one of two outcomes: if the impact velocity is smaller than the mutual escape velocity of the colliding particles, defined as

$$v_{mut,esc} = \sqrt{\frac{G(m_1 + m_2)}{r_1 + r_2}}, \tag{12}$$

where m_1, m_2 and r_1, r_2 are the masses and radii of colliding particles 1 and 2, then the bodies perfectly merge. For impact velocities larger than $v_{mut,esc}$, no mass is transferred, and the bodies undergo a completely elastic bounce. Because there is no possibility of partial accretion, this model likely restricts growth more than the model used by Leinhardt & Stewart (2012). However, we will show below that the bounce-merge model does not meaningfully affect the outcome of the planetesimal accretion phase, and so a partial accretion model should do the same.

For the configuration of initial conditions we have chosen, the typical encounter velocity (defined by $v_{enc} = \langle e^2 \rangle^{1/2} v_k$, where v_k is the local Keplerian velocity) is

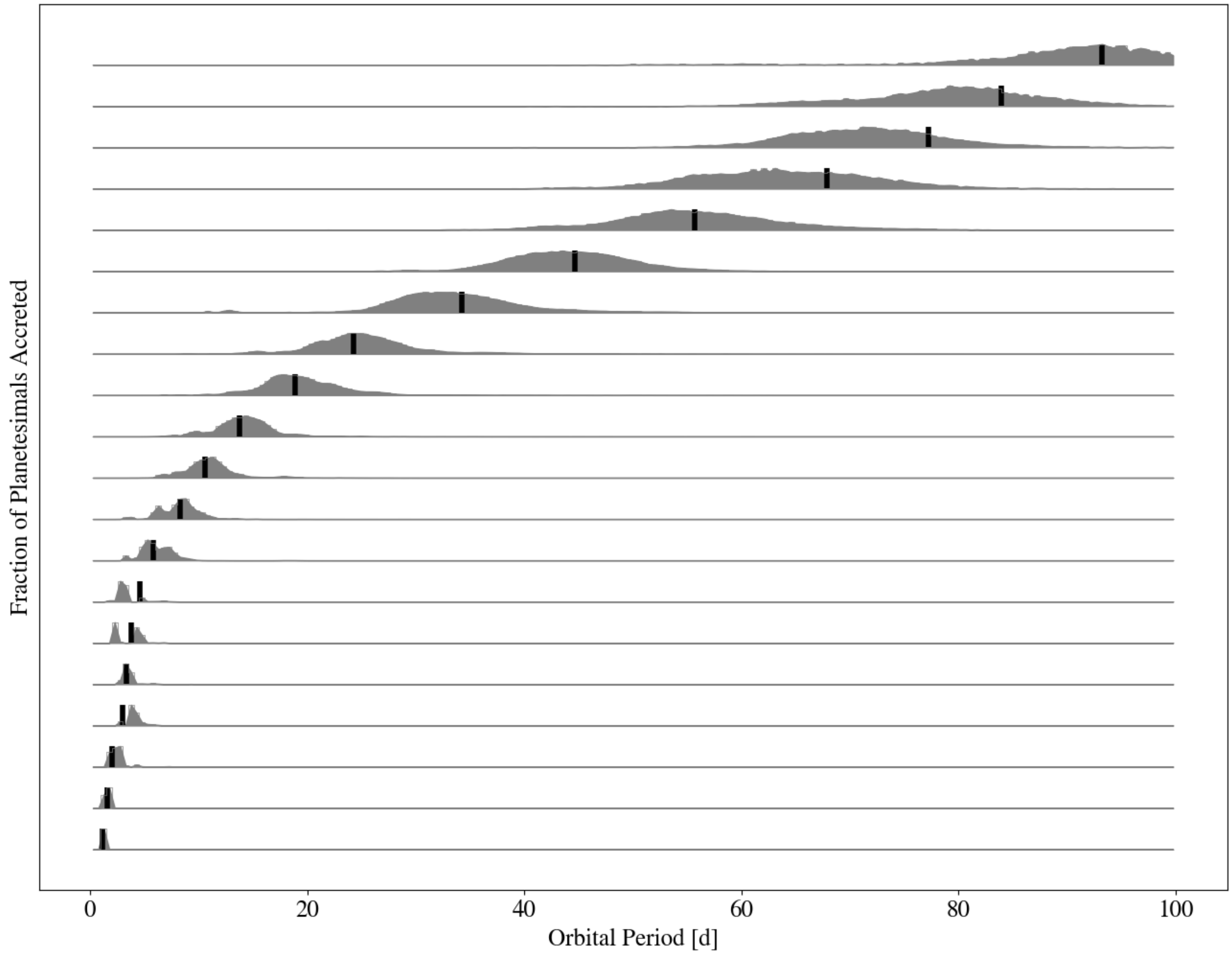

Figure 10. For the 20 most massive bodies at the end of the fdHi simulation, the relative shape of the accretion zones for each body are shown. The black hash marks indicate the present position of the body. The accretion distributions indicate the initial locations of the planetesimals that were used to assemble a body, rather than the locations at which collisions with the massive body occurred.

about 25 percent larger than $v_{mut,esc}$. Because the encounter velocities follow a Gaussian distribution, there should be some small subset of collisions that still meet the merger criteria. In addition, $v_{mut,esc}$ becomes larger as the bodies grow and the merger criteria should become easier to meet as the system evolves.

In figure 12, we show the results of two versions of the fdLo simulation, one with mergers only (shown in orange) and one with the bounce-merge model (shown in green). The blue points in the top panel show the initial conditions used for both cases. Because the bounce-merge model greatly increases the number of timesteps required, we choose to model only the innermost part of the disk to reduce the computational cost. Although the bounce-merge simulation takes much longer to reach the same phase of evolution, the resulting orbits and masses of the embryos are indistinguishable from the merger-only case.

To investigate the differences between the two collision models early in the simulations, we show the time evolution of the ratio between the maximum and mean mass in figure 13. In both cases, this ratio grows at early times, which indicates that runaway growth still operates, regardless of the collision model used. In the bounce-merge case, the mass ratio peaks at a higher value, while also undergoing a longer runaway growth phase. This suggests that the mass distribution becomes much less unimodal during this growth process, but as figure 12 shows, this does not affect the resulting embryos or allow for a residual planetesimal population.

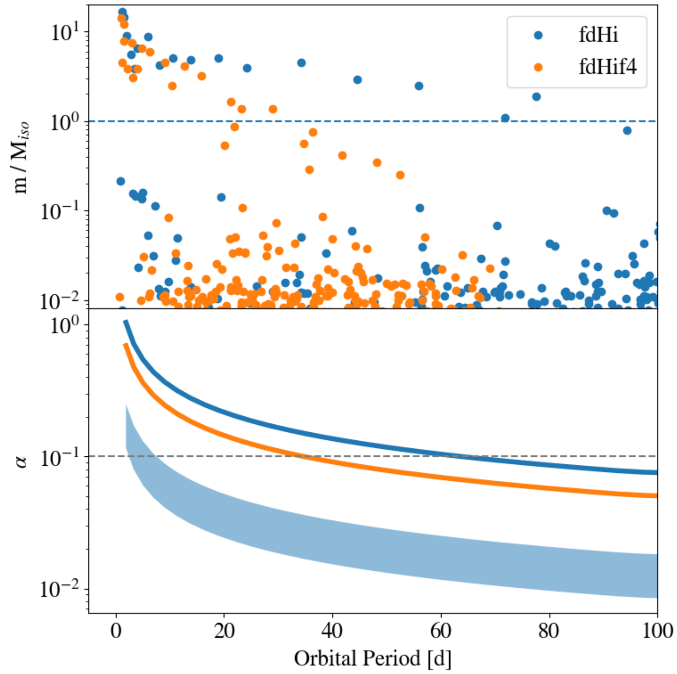

Figure 11. In the top panel, we show the final masses of the bodies from the fdHi and fdHif4 simulations in units of the isolation mass for $\tilde{b} = 2\sqrt{3}$. The bottom panel shows the variation of α with orbital period for the bodies used in each case (solid curves). The orbital period at which $\alpha \simeq 0.1$ matches well with the intersection of the embryo mass distribution and isolation mass. The shaded region in the bottom panel show the values of alpha for realistic-sized ($f = 1$) planetesimals with bulk densities between 10 and 1 g cm^{-3}.

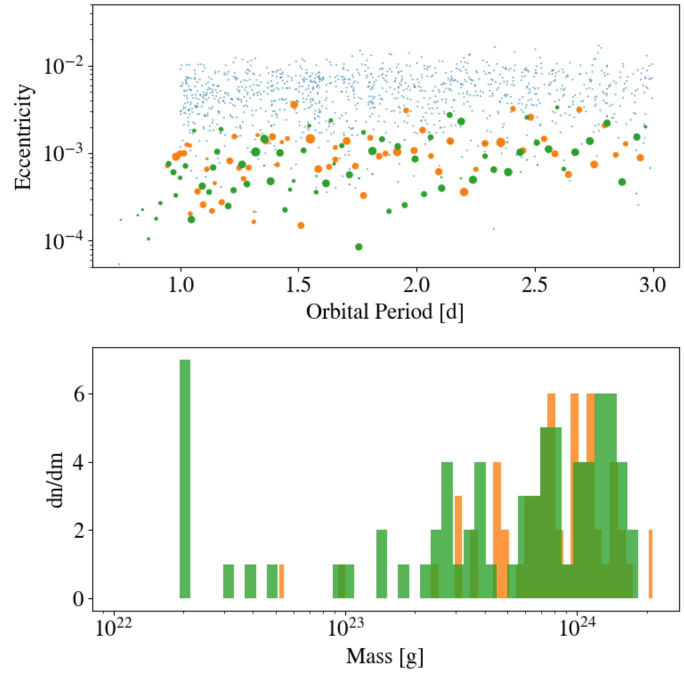

Figure 12. A comparison between the innermost regions of the fdLo (orange) simulation, and a second version using a bounce-merge collision model (green). In the top panel, the period-eccentricity state of the particles is shown, with marker sizes indicating relative mass. The blue points represent the initial state of the simulations. The bottom panel compares the final masses of the bodies.

Radial mixing appears to be enhanced by a partial collision model, along with smaller collision cross section inflation (Childs & Steffen 2022).

6.3. *Type I Migration*

What is the migration timescale for the embryos to move to the inner edge of the disk? Maybe this section isn't terribly important and should be excluded? TRQ: I agree

7. SUMMARY AND DISCUSSION

In this work, we have demonstrated that planetary embryo formation operates in two distinct modes in a planet-forming disk. In the first mode, gravitational feedback from the growing embryos heats the remaining planetesimals and results in a dynamically cold population of embryos with a significant amount of residual planetesimals. This corresponds to the "oligarchic growth" case revealed by (Kokubo & Ida 1998). In the second mode, the gravitational feedback does not operate, embryos quickly sweep up all planetesimals, and grow about twice as large as is predicted by oligarchic growth. The distinction between these modes is determined by ratio between the physical size of the bodies and their Hill radius.

We have demonstrated the outcome of both accretion modes through a sparsely sampled parameter study. The initial planetesimal distribution can be described in terms of two dimensionless constants, α and β, which describe the ratio between the physical radius of the planetesimals and the Hill (r_h) and gravitational (r_g) radii, respectively. For a fixed planetesimal mass and radius, α scales with the orbital period and β scales with the level of dynamical excitation of the disk. We showed that $\alpha \ll 1$ leads to oligarchic growth, while a non-negligible α produces this new non-oligarchic growth mode. We find that the resulting mass distribution, along with the final eccentricities of the embryos and residual planetesimals, ends up the same, regardless of the initial value of β.

So long as the density of the bodies does not significantly change as their mass distribution evolves, this ratio, and therefore the boundary between these accretion modes is set entirely by the distance from the star. Because both the physical and Hill radii of the bodies

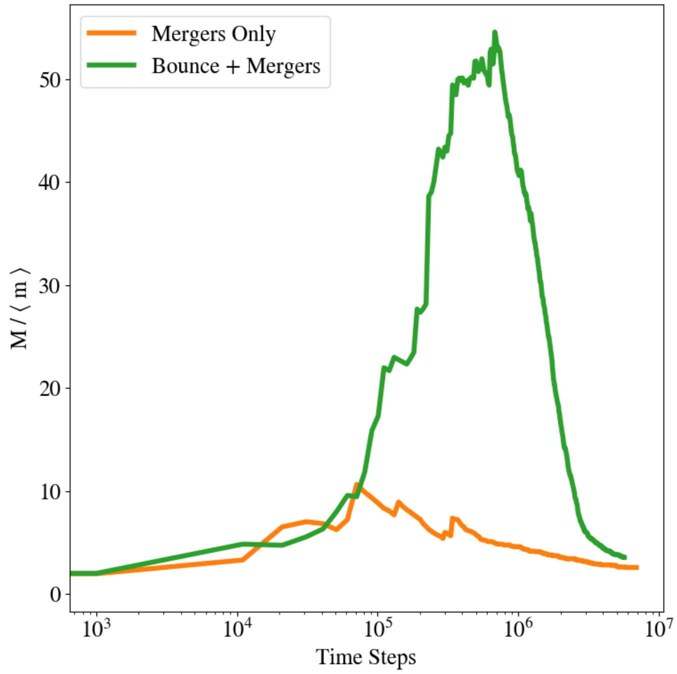

Figure 13. The evolution of the ratio between the maximum and mean mass of the simulations shown in figure 12. In both cases, the system first evolves through a phase of runaway growth, before the massive bodies consume the smaller bodies, driving down the mean mass. With the bounce-merge model, the mass ratio decreases later because not all collisions result in growth.

grows as $M^{1/3}$, the boundary between growth remains at a fixed location in the disk during the planetesimal accretion process.

We have verified this fact by testing the outcome of the planetesimal accretion process for a variety of solid surface density profiles. Although altering the surface density does affect the resulting masses of the embryos, the location of the boundary separating the growth modes is remarkably similar among all of our simulations. We have verified this by comparing the resulting embryo masses to the isolation mass, in addition to highlighting qualitative differences in the accretion history of embryos on both sides of the boundary.

Lastly, we quantified the way in which our use of perfect accretion and an inflated collision cross section, both meant to make the simulations more computationally tractable, affect the non-oligarchic growth mode and the location of the accretion boundary. We showed that although the use of perfect accretion speeds up the growth of the embryos, it does not affect the masses or orbital properties of the resulting bodies. Because the inflated collision cross sections artificially reduce the density of the planetesimals, this shortcut does shift the accretion boundary outward. However, it moves in a predictable fashion and we verified this by running an extra simulation with a modestly smaller collision cross section. In a real planet-forming disk, one would expect this boundary to lie somewhere between 2 and 10 days, depending on the composition of the planetesimals.

To date, there have been no other studies of planetesimal accretion with such a large value of α. However, a value of $\alpha = 1$ corresponds to the Roche limit of a three-body system, and so one might wonder this high-α accretion mode might be relevant for a circumplanetary system. There is a small collection of previous works which use N-body methods to examine in-situ satellitesimal accretion (Ida et al. 1997; Richardson et al. 2000; Ida et al. 2020). Ida et al. (1997) was able to form 1-2 large moons just exterior to the Roche limit, depending on the extent of the disk with very little satellitesimal material left over. The widest disk they modeled extended out to $\alpha = 0.5$. Qualitatively, this result is very similar to the short period planetesimal accretion mode observed in our simulations. Ida et al. (2020) modeled a much wider satellitesimal disk, which extends out to about $\alpha \approx 0.05$. Inside to the $\alpha = 0.1$ accretion boundary (which lies near $15R_U$ in figure 1 of Ida et al. (2020)), bodies grow beyond the isolation mass, while the opposite is true on the other side of the boundary. In addition, a residual population of satellitesimals is still present beyond the boundary, which suggests that oligarchic growth is indeed operating on the far side.

Presently, the implications that this non-oligarchic accretion mode has for the formation of short-period terrestrial planets, and whether the accretion boundary would leave any lasting imprint on the final orbital architecture, is unclear. One point that our results do highlight is that the initial conditions used for most late stage planet formation simulations are overly simplistic. Clement et al. (2020) recently simulated planetesimal accretion in a disk extending from the orbit of Mercury to the asteroid belt and found that the disk never reaches a state in which equally-spaced, isolation mass embryos are present everywhere simultaneously. Instead, different annuli reach a 'giant impact' phase at different times, preventing the onset of a global instability throughout the entire disk, as is common in classic terrestrial planet formation models (Chambers & Wetherill 2001; Raymond et al. 2009).

To connect these accretion modes to the final orbital architecture, and to ultimately determine what implications an in situ formation model has for the growth of STIPs, we will continue to evolve the final simulation snaphots presented here with a hybrid symplectic integrator. The final distribution of planets formed, along with composition predictions generated by applying cosmochemical models to our initial planetesimal distributions and propagating compositions through the merger trees, will be examined in a follow-up paper.

8. ACKNOWLEDGEMENTS

NSF, XSEDE.

REFERENCES

Adachi, I., Hayashi, C., & Nakazawa, K. 1976, Progress of Theoretical Physics, 56, 1756, doi: 10.1143/PTP.56.1756

Andrews, S. M., & Williams, J. P. 2005, ApJ, 631, 1134, doi: 10.1086/432712

Bai, X.-N., & Stone, J. M. 2010, ApJ, 722, 1437, doi: 10.1088/0004-637X/722/2/1437

Barnes, R., Quinn, T. R., Lissauer, J. J., & Richardson, D. C. 2009, Icarus, 203, 626, doi: 10.1016/j.icarus.2009.03.042

Beitz, E., Güttler, C., Blum, J., et al. 2011, ApJ, 736, 34, doi: 10.1088/0004-637X/736/1/34

Birnstiel, T., Fang, M., & Johansen, A. 2016, SSRv, 205, 41, doi: 10.1007/s11214-016-0256-1

Blum, J., & Münch, M. 1993, Icarus, 106, 151, doi: 10.1006/icar.1993.1163

Chambers, J. E., & Wetherill, G. W. 1998, Icarus, 136, 304, doi: 10.1006/icar.1998.6007

—. 2001, M&PS, 36, 381, doi: 10.1111/j.1945-5100.2001.tb01881.x

Childs, A. C., & Steffen, J. H. 2022, MNRAS, 511, 1848, doi: 10.1093/mnras/stac158

Clement, M. S., Kaib, N. A., & Chambers, J. E. 2020, PSJ, 1, 18, doi: 10.3847/PSJ/ab91aa

Colwell, J. E. 2003, Icarus, 164, 188, doi: 10.1016/S0019-1035(03)00083-6

Fabrycky, D. C., Lissauer, J. J., Ragozzine, D., et al. 2014, ApJ, 790, 146, doi: 10.1088/0004-637X/790/2/146

Hansen, B. M. S., & Murray, N. 2012, ApJ, 751, 158, doi: 10.1088/0004-637X/751/2/158

Hayashi, C. 1981, Progress of Theoretical Physics Supplement, 70, 35, doi: 10.1143/PTPS.70.35

Ida, S. 1990, Icarus, 88, 129, doi: 10.1016/0019-1035(90)90182-9

Ida, S., Canup, R. M., & Stewart, G. R. 1997, Nature, 389, 353, doi: 10.1038/38669

Ida, S., Kokubo, E., & Makino, J. 1993, MNRAS, 263, 875, doi: 10.1093/mnras/263.4.875

Ida, S., & Makino, J. 1993, Icarus, 106, 210, doi: 10.1006/icar.1993.1167

Ida, S., Ueta, S., Sasaki, T., & Ishizawa, Y. 2020, Nature Astronomy, 4, 880, doi: 10.1038/s41550-020-1049-8

Jetley, P., Gioachin, F., Mendes, C. Kale, L., & Quinn, T. 2008, Proceedings of IEEE International Parallel and Distributed Processing Symposium

Johansen, A., Blum, J., Tanaka, H., et al. 2014, in Protostars and Planets VI, ed. H. Beuther, R. S. Klessen, C. P. Dullemond, & T. Henning, 547

Johansen, A., Oishi, J. S., Mac Low, M.-M., et al. 2007, Nature, 448, 1022, doi: 10.1038/nature06086

Kokubo, E., & Ida, S. 1996, Icarus, 123, 180, doi: 10.1006/icar.1996.0148

—. 1998, Icarus, 131, 171, doi: 10.1006/icar.1997.5840

—. 2000, Icarus, 143, 15, doi: 10.1006/icar.1999.6237

—. 2002, ApJ, 581, 666, doi: 10.1086/344105

Leinhardt, Z. M., & Stewart, S. T. 2012, ApJ, 745, 79, doi: 10.1088/0004-637X/745/1/79

Lissauer, J. J., & Stewart, G. R. 1993, in Protostars and Planets III, ed. E. H. Levy & J. I. Lunine, 1061

Lyra, W., Johansen, A., Klahr, H., & Piskunov, N. 2008, A&A, 491, L41, doi: 10.1051/0004-6361:200810626

Menon, H., Wesolowski, L., & Zheng, G. e. a. 2015, Computational Astrophysics and Cosmology, 2, 1

Morishima, R., Stadel, J., & Moore, B. 2010, Icarus, 207, 517, doi: 10.1016/j.icarus.2009.11.038

Nakagawa, Y., Sekiya, M., & Hayashi, C. 1986, Icarus, 67, 375, doi: 10.1016/0019-1035(86)90121-1

Nakazawa, K., & Ida, S. 1988, Progress of Theoretical Physics Supplement, 96, 167, doi: 10.1143/PTPS.96.167

Raymond, S. N., O'Brien, D. P., Morbidelli, A., & Kaib, N. A. 2009, Icarus, 203, 644, doi: 10.1016/j.icarus.2009.05.016

Raymond, S. N., Quinn, T., & Lunine, J. I. 2005, ApJ, 632, 670, doi: 10.1086/433179

—. 2006, Icarus, 183, 265, doi: 10.1016/j.icarus.2006.03.011

Raymond, S. N., Scalo, J., & Meadows, V. S. 2007, ApJ, 669, 606, doi: 10.1086/521587

Richardson, D. C. 1994, MNRAS, 269, 493, doi: 10.1093/mnras/269.2.493

Richardson, D. C., Quinn, T., Stadel, J., & Lake, G. 2000, Icarus, 143, 45, doi: 10.1006/icar.1999.6243

Safronov, V. S. 1969, Evoliutsiia doplanetnogo oblaka.

Wallace, S. C., & Quinn, T. R. 2019, MNRAS, 489, 2159, doi: 10.1093/mnras/stz2284

Weidenschilling, S. J. 1977, MNRAS, 180, 57, doi: 10.1093/mnras/180.2.57
—. 1989, Icarus, 80, 179, doi: 10.1016/0019-1035(89)90166-8
Wetherill, G. W., & Stewart, G. R. 1989, Icarus, 77, 330, doi: 10.1016/0019-1035(89)90093-6